Magnetic Field Effects on the Open Circuit Potential of Ferromagnetic Electrodes in Corroding Solutions

Amala Dass,[†] Joseph A. Counsil,[†] Xuerong Gao,[†] and Nicholas Leventis*[,‡]

Department of Chemistry, University of Missouri−Rolla, Rolla, Missouri 65409, and Materials Division, NASA Glenn Research Center, 21000 Brookpark Road, M.S. 49-1, Cleveland, Ohio 44135

Received: December 17, 2004; In Final Form: March 17, 2005

Magnetic fields shift the open circuit potential (OCP) of ferromagnetic electrodes (Fe, Co, and Ni) in corroding solutions. The OCP changes we observe (a) follow the series Fe>Co>Ni; (b) increase with the magnetic flux density; (c) reach a maximum with disk electrodes approximately 1 mm in diameter; and (d) depend on the orientation of the electrode. We report that when the surface of the electrode is oriented parallel ($\theta = 90°$) or perpendicular ($\theta = 0°$) to the magnetic field, the open circuit potential moves in *opposite* directions (positive and negative, respectively) with the largest changes occurring when the electrode surface is parallel to the magnetic field. Nonconvective sleeve electrodes produce the same behavior. The overall experimental evidence suggests that the magnetic field changes the OCP by modifying the surface concentrations of the paramagnetic participants in the corrosion process of the ferromagnetic electrode by species in solution; this in turn is accomplished by imposing a field-gradient driven mode of mass transfer upon paramagnetic species in solution (magnetophoresis). Simulations of the magnetic field around the ferromagnetic electrode at the two extreme orientations considered here show that in one case ($\theta = 90°$) field gradients actually *repel*, while in the other case ($\theta = 0°$) they attract paramagnetic species in the vicinity of the electrode.

1. Introduction

Corrosion is the thermodynamically favorable oxidative degradation of metals. Since metal structures still comprise the cornerstone of civilization, understanding and preventing corrosion is of immense economic importance.[1a] Mechanistically, corrosion can be a very complex process. Experimentally, however, there is an easy-to-follow, nonperturbing system parameter, the open circuit potential.

In the meantime, magnetic effects on the open-circuit potential of metals have been known since the 1880s,[2] and sporadic reports have continued throughout the twentieth century. Most notably, the 1942 thermodynamic study by Koenig and Grinnell on the theory of galvanic cells subjected to magnetic fields concluded that the effect on the electromotive force of ferromagnetic wire electrodes placed parallel to the field should be quite small (6 microvolt in a field of 0.1 T).[3] Earlier reports of much larger magnetically induced potential changes (in the order of 40 mV[4]) were not given much attention. Indeed, from an equilibrium perspective, the magnetic field effect on the electrode potential does appear to be quite small. In the mid 1990s, Yamamoto et al. reported that by switching a 15 T field 'on' at about ambient temperature, ferromagnetic hydride electrodes such as $LaCo_5H_x$ and $Y_2Co_7H_x$ undergo 1.7 mV and 0.5 mV changes in their potential, respectively.[5] These findings were rationalized by introducing a magnetic free energy term in the Nernst equation, and were regarded as a novel method for magnetostatic-to-chemical energy conversion. In 2001, we reported a general expression for the magnetoelectrochemical potential of redox systems where one redox form is paramagnetic; that expression can be used to derive a general magnetic correction term to the Nernst equation,[6] $\Delta\phi = [N_A(m^*)^2/z_jFkT]\Delta(|\boldsymbol{B}|^2)$,[7] from which it is calculated that at $|\boldsymbol{B}| = 1$ T, $\Delta\phi = 0.13\ \mu$V (assuming that the spin is 1/2 and the g factor = 2).

Nevertheless, other recent evidence seems to support the early reports from more than a century ago on magnetic field-induced potential changes on the order of tens of millivolt. In 1996, Waskaas studied the magnetic field effect on the open-circuit potential of various foil electrodes (Fe, Pt, Ni, Zn, and Cu) placed perpendicular to the field in solutions of 'different magnetic properties' ($FeCl_3$, $FeCl_2$, $FeSO_4$, $NiCl_2$, $ZnCl_2$, $CuCl_2$).[8] Only the Fe/$FeCl_3$ electrode/electrolyte system gave any response, which, in fact, could be quite substantial: up to 84.5 mV in the positive direction in a field of 0.81 T with an $FeCl_3$ concentration of 2 M. In subsequent work with Co and Ni electrodes, Waskaas and Kharkats reported similar results but in the opposite (negative) direction.[9] The observed phenomena were associated with the paramagnetic properties of the solution, suggesting that paramagnetic species reacting with the electrode produce concentration gradients (and therefore susceptibility gradients), which in turn gave rise to concentration-gradient paramagnetic forces that produce "magnetoconvection." In our opinion, a basic problem with this mechanism is that the reaction product of the comproportionation reaction between Fe with Fe^{3+} is the high-spin paramagnetic Fe^{2+},[10] hence the susceptibility of the solution should in fact increase toward the electrode rather than toward the solution, and therefore the paramagnetic force should be directed toward the electrode causing retention of the solution, not convection.[11] The Waskaas system was revisited by Perov et al. who confirmed the results with the Fe electrodes but reported no magnetic effects with the Co and Ni electrodes,[12] and by Hinds et al. who reported orientation-dependent, always positive open circuit potential (OCP) changes in the range of 20−60 mV for

* Corresponding author. Tel.: (216) 433-3202; E-mail: Nicholas.Leventis@nasa.gov

[†] University of Missouri−Rolla.

[‡] NASA Glenn Research Center.

10.1021/jp0442495 CCC: $30.25
Published on Web 05/10/2005

the rest potential of Fe electrodes in paramagnetic solutions of $FeCl_3$ and $Fe(NO_3)_3$, while smaller, also positive shifts (~2 mV) were also observed with Co and Ni electrodes.[13] Nevertheless, based on a comparison of the concentration-gradient paramagnetic force with the driving force for diffusion these authors questioned Waskaas' mechanism,[13] and they offered an alternative explanation based on the fact that ferromagnetic materials bend the magnetic field, generating field gradients that produce field-gradient paramagnetic body forces.[14] But again, with a higher concentration of paramagnetic species closer to the electrode, it is doubtful that field-gradient paramagnetic body forces, being stronger closer to the electrode and fading away toward the bulk, would be able to set the solution in motion.[15]

Although an exact mechanism has not yet been established, there appears to be a consensus on the non-equilibrium origin of the open circuit potential changes induced by the magnetic field, and particularly on the fact that mass transfer driven by interfacial chemical reactions plays a pivotal role. However, special significance seems to be attributed to the bulk paramagnetic properties of the solution in contact with the ferromagnetic electrode, but as it turns out from this study here, the key property of the solution side of the interface is only the corroding nature of that solution: carefully chosen *diamagnetic* corroding solutions using $[Co(bipy)_3](ClO_4)_3$ as the oxidizing agent (bipy = 2,2′-bipyridine) produce a similar response to that from the Fe/Fe^{3+} system. Furthermore, corrosion of metals in aqueous solutions can be followed by formation of oxides and films,[16] whose chemical and magnetic properties may complicate the magnetic response of the system.[17] These processes were controlled by working in CH_3CN solutions and thus the principal question was shifted to whether open circuit potential changes are caused indeed by convection, as suggested by Waskaas[8,9] and by Hinds et al.,[13] and if so, to find the responsible forces. For this purpose we have conducted experiments using nonconvective 'sleeve' electrodes, whose behavior outside the magnetic field is controlled by diffusion. Overall, our data establish that the main contributor in the observed magnetic phenomena is field-gradient driven transport of magnetic dipoles (magnetophoresis).[18] Detail studies of the OCP as a function of the electrode orientation in the magnetic field reveal *opposite* responses for electrodes with their surfaces oriented parallel versus perpendicular to the field. This behavior has not been reported before and we trace it through magnetostatic calculations using ANSYS to the distinctly different shape of the magnetic field in the vicinity of the ferromagnetic disk electrode in the two orientations.

2. Experimental Section

Materials. Anhydrous CH_3CN, nitrobenzene, and $LiClO_4$ were purchased from Aldrich. $LiClO_4$ was dried by heating overnight at 80 °C under vacuum. Nitrobenzene was distilled. Tetrabutylammonium perchlorate (TBAP) was synthesized and dried as described before.[19a] $[Co(bipy)_3](ClO_4)_3 \cdot 3H_2O$ and $[Co(bipy)_3](ClO_4)_2$ were synthesized by a modification of a literature procedure[19b] and were available from our previous studies.[15,20]

Equipment. Working electrodes were made with Fe, Co, Ni, Zn, Pt, and Au metal wires. All wires were purchased from Alfa-Aesar (Ward Hill, MA) unless noted otherwise at the highest purity available.[21] Bent working electrode assemblies (Scheme 1A) were constructed as follows.[22] Glass tubes of appropriate inner diameter to hold the wires were heat-bent ~1 cm from their ends. (Bent electrodes are used to orient the electrode surface parallel or perpendicular with respect to the magnetic field.) For electrical contact, thin Cu wires 25 μm in diameter were wound tightly around the end of short (~5 mm) wires of each electrode material. Then white epoxy glue (Hysol 1C, Dexter Corporation, Seabrook, NH) was applied to hold the electrodes in place inside the bent end of the glass tube. The epoxy was cured at 60 °C overnight. The side of the working electrode to be exposed to the solution was polished first with fine sandpaper and then successively with 6, 3, and 1 μm diamond paste on DR−Nap polishing cloth (Struers, Westlake, OH). Polished electrodes were sonicated in methanol and then air-dried before use.

SCHEME 1: (A) Bent and (B) Nonconvective 'Sleeve' Electrode

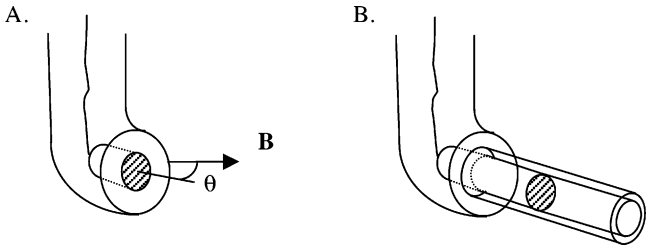

Nonconvective sleeve electrodes (Scheme 1B) were constructed by a method similar to regular working electrodes, except that the metal wire is left to protrude outside the glass tube by ~5 mm. The protruding part of the wire was polished and cleaned as before, and HPLC plastic tubing of the appropriate diameter was fitted to this protruding wire so that it extends ~2 mm beyond its edge. This electrode does not allow convection, restricting mass transfer to diffusion-like processes.

Open circuit potential data were recorded with a Kipp & Zonen X,Y,Y′,T recorder versus an aqueous Ag/AgCl/KCl (3M) reference electrode purchased from CH Instruments (Austin, TX).

Magnetic field was generated by an electromagnet constructed around two iron pole pieces, 9 cm in diameter extending 4.5 cm out of the Cu coils and leaving a gap of 3 cm. The two poles were mounted with iron posts on a 2 in. thick iron base plate. The coils were powered with a Kepco Inc. (Flushing, NY) power supply, model JQE 150−1.5, with maximum DC current output of 1.5 A. The intensity of the magnetic field was measured with a Gauss meter model GM1A manufactured by Applied Magnetics Laboratory, Inc. (Baltimore, MD). With the power supply at the maximum DC current output of 1.5 A, the field generated in the gap between the centers of the two poles is 3.3 T. The field was 3.24 T one inch away from the center of the poles (a 1.8% decrease). Thus, it is calculated that the magnetic field strength across the diameter (1.00 mm) of disk electrodes placed near the center of the gap between the poles of the electromagnet and facing the magnetic field is, for all practical purposes, homogeneous within 0.23%.

Methods. All glassware were rinsed with acetone, washed with Micro cleaning solution, rinsed with copious amounts of distilled water, and dried at 60 °C. All magnetoelectrochemical experiments were carried out in test tubes (16 cm long, 2.25 cm in diameter) or Wheaton scintillation vials (Fisher) containing 5−10 mL of the appropriate electrolytic solution under an Ar blanket. All experiments were carried out at 23−25 °C. The magnetic flux density, $\boldsymbol{B}$, was adjusted by varying the power supply current, and the field was switched on and off using the power supply switch. The corresponding open circuit potential of the metal electrode was recorded using the XY recorder. Three electrodes of each kind were made and experiments were repeated several times for reproducibility. Placement of the reference electrode outside the magnetic field, using a salt bridge

connection, did not show any difference in the open circuit potential versus time plot. Hence the reference electrode was left in the same cell with the magnetic field.

Finite element electromagnetic simulations were performed and results were plotted using ANSYS 6.2 (Cannonsburg, PA). A model of our system was built as follows (also refer to the Supporting Information). Two permanent magnets with accompanying iron pole pieces were created to simulate the externally applied homogeneous magnetic field. An air gap was present between them and a small ferromagnetic cylinder was placed at the center. The base of that cylinder comprises the disk electrode. SOLID 98 Brick was the element type, and appropriate material properties were assigned for all the parts of the model. The magnetization of the permanent magnets in the model was adjusted to produce ~3.3 T of a homogeneous field in the gap in order to match the highest field we have been using experimentally. After meshing the model, boundary conditions were applied and the model was solved in three dimensions. (Since at the $\theta = 90°$ orientation there are no symmetry elements at the surface of interest, the base of the ferromagnetic cylinder, the model had to be solved in three dimensions.) Two-dimensional cross-sections were plotted. The results were invariant of the mesh size.

Open circuit potential traces were scanned from the graph paper output of the XY recorder. Background lines were removed and contrast was adjusted in Adobe Photoshop 7.0 (San Jose, CA). Data plotting was done using Origin 6.1 (Northampton, MA).

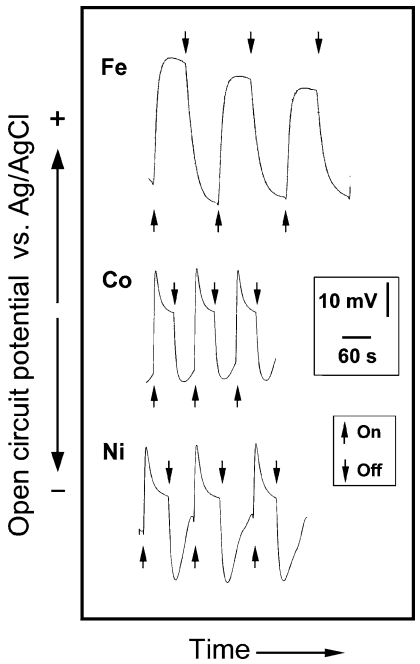

Figure 1. OCP changes with Fe, Co, and Ni electrodes (1 mm diameter) by 'on−off' switching of a 3.3 T magnetic field. The electrode surfaces were oriented parallel to the ***B*** vector ($\theta = 90°$). The electrolytic solution in the case of Fe was based on CH_3CN/H_2O (5:1, v/v), while in the case of Co and Ni on pure CH_3CN. All solutions contained 0.5 M $LiClO_4$ and 3 mM of each of the two forms of $[Co(bipy)_3]^{3+/2+}$.

3. Results and Discussion

3.1. Phenomena to Be Analyzed. The open circuit potential of three freshly polished and dried ferromagnetic disk electrodes (Fe, Co, Ni) was recorded with reference to an aqueous Ag/AgCl electrode in the presence and absence of a 3.3 T magnetic field, in solutions containing 3 mM of both forms of the redox couple $[Co(bipy)_3]^{3+/2+}$ together with 0.5 M $LiClO_4$. (Although control experiments with only one redox form of the complex were run numerous times (see below), it was preferred to include both redox forms in the solution in order to define a fixed point of departure for the OCP: the redox potential of the Co complex.) The solvent in the case of Co and Ni was pure CH_3CN, while in the case of Fe it was a mixture of CH_3CN/H_2O, 5:1 v/v. The electrode was bent, so that the effect of the orientation relative to the ***B*** vector could be tested easily. Maximum effects were observed when the electrode surfaces were parallel to the magnetic field ($\theta = 90°$), and typical data are shown in Figure 1. In agreement with Hinds et al.,[13] all three electrodes gave potential changes in the positive direction when the magnetic field was applied. Fe gave the highest change, ~50 mV (from baseline to steady-state), followed by Co, ~20 mV, and by Ni, ~7 mV. Although specific features may vary, the main dynamic response of the three electrodes to the magnetic field is quite similar: the OCP reaches a maximum quickly and then it relaxes to a steady state, which is maintained for at least 5 min. When the field is turned off, the OCP returns back near to the original baseline. It is noted, however, that all baselines drift, and in this regard the Fe baseline drifts more than those of Co and Ni. In addition, the response of the Fe electrode seems to decline gradually, while the response of the Co and Ni electrodes is significantly more stable. Visual examination of the electrodes after several minutes in the $[Co(bipy)_3]^{3+/2+}$ solution shows that on one hand Co and Ni electrodes no longer have a polished appearance, meaning that they corrode, but they still look metallic, while on the other hand, Fe electrodes develop thin uniform brownish-red films. Qualitatively, the slow decline in the response of the Fe electrode seems to be associated with the appearance of that film, which in turn seems related to the presence of water in our Fe experiments, in agreement with similar observations made by Hinds et al. in aqueous solutions of ferric chloride and nitrate.[13] (Note that unlike Co and Ni, using pure CH_3CN as solvent in the case of Fe seems to prevent the magnetic response of the OCP, presumably due to some sort of passivation of the electrode. By the same token, however, since Co and Ni produced satisfactory response in CH_3CN, they were not tested in the CH_3CN/H_2O mixture.)

Several control experiments were run in parallel to those summarized in Figure 1. Noble metal electrodes of Au and Pt give no response to the magnetic field under the same conditions. Similarly, a corroding diamagnetic Zn electrode did not give any response to the magnetic field, although it does show clear signs of corrosion. The actual electrode potential of the Au or the Pt electrode in the equimolar solution of the two redox forms $[Co(bipy)_3]^{3+}$ and $[Co(bipy)_3]^{2+}$, is always near the electrode potential of the $[Co(bipy)_3]^{3+/2+}$ couple ($E_{1/2} = 0.222$ V vs aq Ag/AgCl).[20] However, the potential of the Fe, Co, and Ni electrodes varies in the range of −0.2 to 0.1 V vs Ag/AgCl, which falls between the electrode potentials of $Fe^{2+/0}$ (−0.64 vs aq Ag/AgCl), $Co^{2+/0}$ (−0.474 V vs aq Ag/AgCl), and $Ni^{2+/0}$ (−0.454 vs aq Ag/AgCl) on one hand,[22c] and the potential of the $[Co(bipy)_3]^{3+/2+}$ couple on the other. Such mixed potentials are characteristic of systems undergoing corrosion.[1b] Indeed, an identical response was obtained from all three ferromagnetic electrodes when only oxidizing diamagnetic $[Co(bipy)_3]^{3+}$ was included in the solution, and no response was obtained when only paramagnetic $[Co(bipy)_3]^{2+}$ was used. On the other hand, the absence of response from corroding diamagnetic Zn electrodes signifies that corrosion and production of paramagnetic species, although necessary, are not sufficient conditions in order to elicit magnetic response from the OCP of a metal. Corrosion

of Zn does produce paramagnetic $[Co(bipy)_3]^{2+}$ at the electrode surface, but Zn is not ferromagnetic, which, therefore, seems to be a prerequisite for magnetic response. Thus, all indicators so far show that corrosion and production of paramagnetic species at a ferromagnetic electrode surface, as opposed to the magnetic properties of the bulk solution, are the critical factors for observing open circuit potential changes in the magnetic field. At this point, taking into consideration the high purity metals used for making the electrodes,[21] it is reasonable to assume that all three ferromagnetic electrodes of this study corrode uniformly by the Wagner and Traud mechanism,[1b] according to

$$Fe + 2\ Co^{III} \rightarrow Fe^{2+} + 2\ Co^{II} \quad (1)$$

$$Co + 2\ Co^{III} \rightarrow Co^{2+} + 2\ Co^{II} \quad (2)$$

$$Ni + 2\ Co^{III} \rightarrow Ni^{2+} + 2\ Co^{II} \quad (3)$$

where Co^{III} and Co^{II} stand for the two redox forms of the $[Co(bipy)_3]^{3+/2+}$ couple. (In the case of Fe, there is an additional process that involves formation of oxide, but since it seems that this is a slower process, it will be ignored for the purposes of this study.) The potential that is sampled by the Fe, Co, or Ni electrode is the emf of the corresponding hypothetical cell reaction and is given by eq 4,

$$E = E^0 + \frac{RT}{2F}\ln\frac{(a^s_{Co^{III}})^2}{(a^s_{Co^{II}})^2(a^s_{M^{2+}})} + \frac{Q_{M^{2+}}}{2F}|\boldsymbol{B}|^2 + \frac{Q_{Co^{II}}}{F}|\boldsymbol{B}|^2 \quad (4)$$

where M^{2+} stands for Fe^{2+}, Co^{2+}, or Ni^{2+} and where the two Q's are constants that depend on the magnetic moments of the corresponding species (see Appendix). It is calculated that the contribution of the magnetic terms at room temperature, even at $|\boldsymbol{B}| = 3.3$ T and for Fe^{2+}, whose magnetic moment is 5.2 μ_B,[10] is not more than 0.2 mV. Thus, changes in the OCP observed upon application of the magnetic field should be attributed to an alteration of the activities, $a^s_{M^n}$ (M^n: Co^{II}, Co^{III}, and M^{2+}) of paramagnetic Co^{II} and Fe^{2+} *at the electrode surface*, via modification of their rates of mass transfer. The emphasis of our inquiry is then shifted to identify the specific mode of mass transfer that is affected by the magnetic field in our system. We begin by reviewing the possible magnetic effects on mass transfer.

3.2. Brief Review of Mass Transfer in the Magnetic Field. The flux $\boldsymbol{J}_j$ of a charged magnetic dipole j is given by eq 5

$$\boldsymbol{J}_j = -D_j\nabla C_j - (z_jC_jD_jF/N_Akt)\nabla\phi + 2C_jD_j(m^*/kT)^2\boldsymbol{B}\cdot\nabla\boldsymbol{B} + C_j\boldsymbol{v} \quad (5)$$

where C_j and D_j are the concentration and the diffusion coefficient of j, respectively, and all other symbols, except $\boldsymbol{v}$, have their previously defined meanings.[7] The first term of eq 5 represents diffusion, the second migration (flux due to electric fields), the third magnetophoresis (flux of magnetic dipoles driven by magnetic field gradients), and the last convection by movement of the volume element of the solution that contains j.

Magnetic effects in the flux of j may be expressed via magnetophoretic transport, or after momentum transfer via the body forces that control the evolution of the velocity profile $\boldsymbol{v}$ as required by the Navier−Stokes equation (Newton's second law of motion in an incompressible fluid):

$$\rho\left(\frac{\partial}{\partial t} + \boldsymbol{v}\cdot\nabla\boldsymbol{v}\right) = -\nabla P + \eta\nabla^2\boldsymbol{v} + \boldsymbol{g} + \boldsymbol{F}_{mag} \quad (6)$$

The left-hand term of eq 6 represents mass × acceleration per unit volume (ρ: density), while the right-hand term is the sum of all possible forces on the volume element: hydrostatic pressure (P), friction (η: viscosity), gravity ($\boldsymbol{g}$), and the magnetic body forces, respectively. The magnetic force $\boldsymbol{F}_{mag}$ is the sum of the magnetohydrodynamic (Lorenz) force, $\boldsymbol{F}_{MHD}$, and the two paramagnetic body forces $\boldsymbol{F}_{\nabla B}$ and $\boldsymbol{F}_{\nabla C}$:[6,15]

$$\boldsymbol{F}_{mag} = \boldsymbol{F}_{MHD} + \boldsymbol{F}_{\nabla B} + \boldsymbol{F}_{\nabla C} \quad (7)$$

$\boldsymbol{F}_{MHD}$ arises from moving charges (cations and anions) in the magnetic field and is given as the cross-product of the current density and the magnetic induction, $\boldsymbol{i} \times \boldsymbol{B}$. The field-gradient paramagnetic force, $\boldsymbol{F}_{\nabla B}$, is proportional to $C_j\boldsymbol{B}\cdot\nabla\boldsymbol{B}$ and moves volume elements containing paramagnetic species toward regions of higher magnetic flux density. The concentration gradient paramagnetic force, $\boldsymbol{F}_{\nabla C}$, is proportional to $|\boldsymbol{B}|^2\nabla C_j$ and moves volume elements containing concentration gradients of magnetic dipoles in the direction of increasing concentration of j. A frequent source of confusion is that $\boldsymbol{F}_{\nabla B}$ and the magnetophoretic mode of mass transfer both depend on $\boldsymbol{B}\cdot\nabla\boldsymbol{B}$. However, it should be apparent at this point that magnetophoretic transport concerns individual magnetic dipoles j and is a mode of mass transfer analogous to diffusion and electrophoretic migration. On the other hand, $\boldsymbol{F}_{\nabla B}$ is a body force that moves the solution that contains dipoles, causing convection. To illustrate this point, we refer in passing to the following simple experiment that differentiates between volume movement caused by $\boldsymbol{F}_{\nabla B}$ and the magnetophoretic mode of mass transfer. As a model for a volume element in the continuum, we have considered a vial filled with an isotropic suspension of iron powder in a viscous liquid (e.g., mineral oil). If the vial approaches the gap of a strong electromagnet, it will "fly" out and stick on one of the poles. A quick look inside the vial shows individual particles still "migrating" toward the end of the vial closer to the pole. The force that pulls the vial toward the magnet is $\boldsymbol{F}_{\nabla B}$; the slower movement of particles is magnetophoresis.

Since our experiments involve open circuit conditions, there is no current passing through the system ($\boldsymbol{i} = 0$; see Supporting Information), and therefore there are no magnetohydrodynamic forces to be considered ($\boldsymbol{F}_{MHD} = 0$). So the inquiry is focused on whether magnetic effects on the OCP are due to (a) convection owing to the remaining body forces $\boldsymbol{F}_{\nabla B}$ and $\boldsymbol{F}_{\nabla C}$, or (b) magnetophoresis. This is to be decided from studies of the system response as a function of various experimental variables. Those variables are $|\boldsymbol{B}|$, the size of the electrode, the orientation of the electrode relative to the magnetic field, and the use of nonconvective 'sleeve' electrodes. Certain conclusions we are forced into with regard to the shape of the magnetic field are confirmed by simulation. Results point toward magnetophoresis as the controlling mode of mass transfer. To provide final supporting evidence for the proposed mechanism, it was necessary to deconvolute "chemically" the solution side of the mechanism from the electrode side. That was accomplished by following the fate of electrogenerated nitrobenzene anion radicals under identical experimental conditions.

3.3. Effect of the Magnetic Field and the Size of the Electrode on the Open Circuit Potential. Figure 2 demonstrates the effect of the magnetic flux density, $|\boldsymbol{B}|$, on the OCP of three Fe disk electrodes with different diameters (1.5, 1.0, and 0.5 mm) under the conditions of Figure 1. Clearly, in the range of $|\boldsymbol{B}|$ considered, the magnitude of the OCP increases

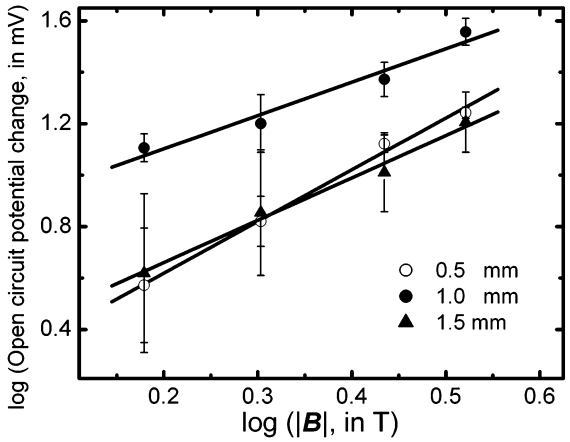

Figure 2. The effect of the magnetic flux density $|\boldsymbol{B}|$ of a homogeneous magnetic field on the OCP of Fe disk electrodes in CH_3CN/H_2O (5:1, v/v)/0.5 M $LiClO_4$ solutions containing ~3 mM of each of the redox forms of $[Co(bipy)_3]^{3+/2+}$. The surfaces of the electrodes were oriented parallel ($\theta = 90°$) to $\boldsymbol{B}$. (Electrode diameters are reported in the figure. For the 0.5 mm electrode: slope = 2.01; intercept = 0.22; $R^2 = 0.99$. For the 1.0 mm electrode: slope = 1.30; intercept = 0.84; $R^2 = 0.98$. For the 2.0 mm electrode: slope = 1.64; intercept = 0.33; $R^2 = 0.99$.)

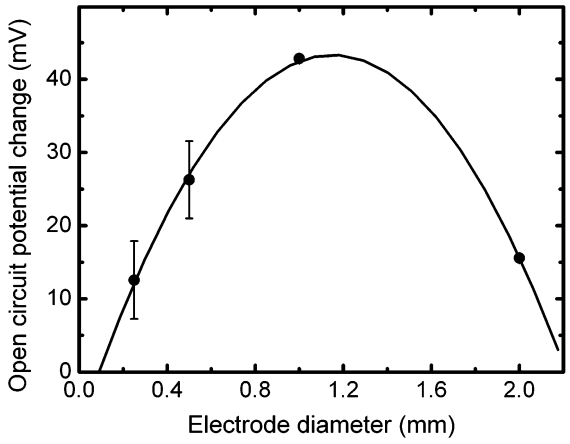

Figure 3. The effect of the electrode size on the OCP of Co disk electrodes in an applied field of $|\boldsymbol{B}| = 3.3$ T in CH_3CN/0.5 M $LiClO_4$ solution containing ~3 mM of each of the redox forms of $[Co(bipy)_3]^{3+/2+}$. The surfaces of the electrodes were oriented parallel ($\theta = 90°$) to the magnetic field vector, $\boldsymbol{B}$. (The error bars in the last two data points are within the points themselves.)

as a function of $|\boldsymbol{B}|$. The plots of log(OCP) vs log($|\boldsymbol{B}|$) are linear, although the slopes have no obvious physical significance. The intercept of the 1 mm electrode is higher than the others, indicating that these electrodes produce higher open circuit potential changes in the magnetic field. That correlation between the size of the electrode and the field-induced OCP change is emphasized further in Figure 3 that shows typical data obtained with, for example, Co electrodes placed parallel to the magnetic field under the conditions of Figure 1. Again, at fixed $|\boldsymbol{B}|$, the open circuit potential difference reaches its maximum with 1 mm electrodes. Now, since the corroding electrodes are ferromagnetic, they bend the magnetic field producing field gradients.[14] Therefore, the fact that we observe variations in the OCP with the diameter of the electrode implies that $\boldsymbol{B}\cdot\nabla\boldsymbol{B}$ plays a major role in the OCP changes via either one or both $\boldsymbol{F}_{\nabla B}$ and a magnetophoretic mode of mass transfer (through the third term of eq 5). Qualitatively, the presence of a maximum in the curve of Figure 3 is reconciled by the fact that the smaller the electrode, the more it bends the magnetic field and the stronger the field gradients it generates. On the other hand, the smaller

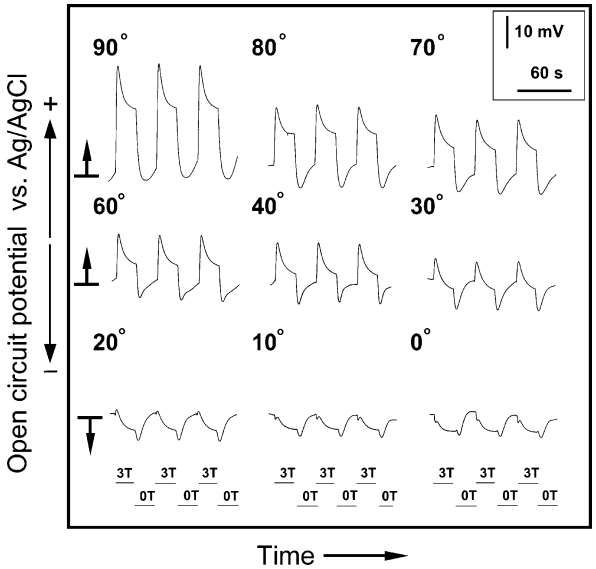

Figure 4. OCP changes with a Co disk electrode (1 mm diameter) by "on−off" switching a 3.3 T magnetic field at different orientations with respect to the direction of $\boldsymbol{B}$, in a CH_3CN/0.5 M $LiClO_4$ solution containing ~3 mM of each of the redox forms of $[Co(bipy)_3]^{3+/2+}$. At 90° the electrode surface is parallel, and at 0° it is perpendicular to the $\boldsymbol{B}$ vector. The arrows at the beginning of each row of data show the direction of the potential shift when $\boldsymbol{B}$ is turned 'on.' Note that at the two extreme orientations the OCP changes in response to $\boldsymbol{B}$ are in opposite directions.

the electrode, the smaller the surrounding space that is affected magnetically. Ultimately, field-gradient related modes of mass transfer would depend on the magnitude of the $\boldsymbol{B}\cdot\nabla\boldsymbol{B}$ vector throughout the entire diffusion layer. Typically, a magnetized ferromagnetic wire affects its environment within a distance about equal to one diameter (see section 3.6 below). On the other hand, for experiments such as those of Figures 1−3, which typically last 3−5 min, it is calculated (using the random walk equation and the diffusion coefficient of the Co^{II} complex in CH_3CN/0.1 M $LiClO_4$,[22d] $\boldsymbol{D}_{Co^{II}} = 6.0 \times 10^{-6}$ cm^2 s^{-1},[20]) that the extent of the diffusion layer is on the order of 0.5−0.6 mm, namely larger than the diameters of the smaller electrodes used in this study and close to the diameter of the electrode that shows the maximum response.

Having concluded that magnetically induced OCP changes depend on field gradients ($\boldsymbol{B}\cdot\nabla\boldsymbol{B}$) invites an investigation of the role of the electrode orientation. After all, at the two extreme orientations of Scheme 1A, the general direction of mass transfer (always toward the electrode) would be parallel to the magnetization of the wire in one case (at $\theta = 0°$) and perpendicular in the other (at $\theta = 90°$). In this regard, the fact that the strongest effects are observed in the latter orientation was rather counterintuitive.

3.4. Effect of the Electrode Orientation on the Open Circuit Potential. In agreement with Hinds et al. (see Introduction),[13] by changing the orientation of the electrode surface relative to $\boldsymbol{B}$ from parallel ($\theta = 90°$) to perpendicular ($\theta = 0°$), the OCP change is reduced by a factor of 3−6. However, we also found that at $\theta = 0°$ the OCP moves in the opposite (negative) direction from where it moves at $\theta = 90°$ (Figure 4). This fact is easy to miss because exact alignment at $\theta = 0°$ is difficult. In our case here, we were able to make this observation as a result of our attempt to follow the evolution of the OCP change from $\theta = 90°$ to $\theta = 0°$ by changing θ gradually, 10° at a time. (Ultimately, the best way to align a ferromagnetic electrode at $\theta = 0°$ is by letting it be aligned by the field.)

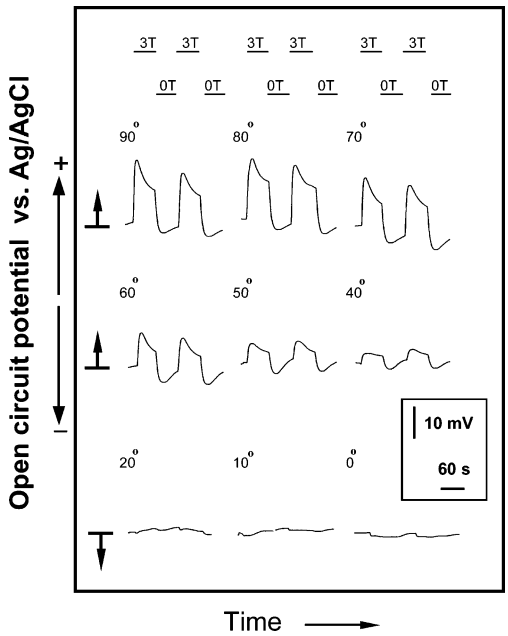

Figure 5. Conditions identical to those of Figure 4, with the exception that the data were obtained with the 'sleeve' electrode (refer to Scheme 1).

Thus, upon close examination of Figure 4, we make the following observations. By applying a field parallel to the electrode surface ($\theta = 90°$), we clearly notice two different regions: a 'fast rise' region, where the open circuit potential increases rapidly, followed by a 'slow decrease' region, where the OCP relaxes to a steady state. As we change the orientation from 90° to 30° with respect to $\boldsymbol{B}$, we observe that the size (magnitude) of the 'fast rise' region decreases significantly, while the magnitude of the 'slow decrease' region decreases minimally. As we move through 10° to the 0° orientation, we notice that the old 'fast rise' region disappears completely, while the old 'slow decrease' region is still present, albeit somewhat smaller in size.

These observations, taken together with the results in section 3.3, lead us to conclude that two possible magnetically induced mass transfer processes should be involved. In principle, either or both of those two modes could be convective or magnetophoretic. However, the change of the OCP in opposite directions at the two extreme orientations rules out a convective contribution in at least one of the two extreme orientations. This is because convection would always refresh the solution in contact with the electrode, so if convection were involved in all instances, then, irrespective of the orientation, the potential would move in the same (positive) direction. Indeed, stirring the solution at both orientations of the electrode relative to $\boldsymbol{B}$ causes a positive shift of the OCP, as expected from the response of eq 4 to a reduction of the value of $(a^{s}_{Co^{II}})^2(a^{s}_{M^{2+}})$. Having to exclude convention, even from only some cases, has to be confirmed independently, and for this purpose we employed nonconvective sleeve electrodes (Scheme 1B) and we conducted experiments identical to those of Figure 4.

3.5. Effect of the Orientation of a Nonconvective 'Sleeve' Electrode on the OCP. By restricting flow of the solution in the radial direction, sleeves also prevent axial flow, because there is no way to fill the void that would be created by such flow. So the only possible modes of mass transfer within the sleeve are diffusion, migration, and magnetophoresis. (Voltammetry with our sleeve electrode under conditions where convective quasi steady-state behavior would be normally expected gives a diffusion-controlled wave.) Thus, Figure 5 shows the OCP response as a function of orientation of a nonconvective 'sleeve' Co electrode (1 mm dia.) with respect to the direction of $\boldsymbol{B}$. By comparison with Figure 4, this electrode reproduces all features observed with the regular disk electrode, including the change in direction of the potential change at the two extreme orientations. The magnitude of the OCP change is smaller compared to Figure 4. This could be attributed to the restricted access to the surface of the electrode through the axial direction only, while field gradients are stronger at the edges.[15] Since convection is not possible with this type of electrode, the results of this experiment comprise strong supporting evidence in favor of field-gradient driven transport of magnetic dipoles (eq 5, third term, magnetophoresis) as the controlling mode of mass transfer in all orientations.

Even within one mechanism, magnetophoresis, there should be two possible scenarios, one allowing for the potential increase at $\theta = 90°$ and one for the potential decrease at $\theta = 0°$. By inspection, eq 6 shows that in order for the potential to increase, the surface concentrations of paramagnetic M^{2+} and $[Co(bipy)_3]^{2+}$ should decrease, i.e., the induced magnetic field should repel these ions away from the surface of the ferromagnetic electrode. By the same token, in order for the potential to decrease, the magnetic field should attract these ions. The only way for this to happen is if the magnetic field is stronger away from the ferromagnetic wire at $\theta = 90°$, and weaker at $\theta = 0°$. The latter situation is rather well known.[7,14,15] The former situation, however, is rather uncommon and we had to resort to calculations.

3.6. Magnetic Field Simulations − Proposed Mechanism. The magnetic field around a short cylindrical ferromagnetic wire (3 mm in length, 1 mm in diameter) was calculated using ANSYS. The dimensions of the wire were chosen to match those of the actual wires cut and embedded in epoxy in order to make the electrodes. We considered two different orientations, one where the axis of the wire is parallel to the magnetic field (corresponding to the $\theta = 0°$ orientation) and one where the base of the cylindrical wire is parallel to the magnetic field (corresponding to the $\theta = 90°$ orientation). Color-coded contour plots for the two orientations are shown in Figure 6. Qualitatively, the magnetic flux density, and by association its gradients, is very different in the two cases. This is especially true at the base of the wire, which is the point of interest in our system. In turn, Figure 7 shows the variation of $|\boldsymbol{B}|$ as a function of distance from the exposed disk to the bulk, where the magnetic flux density matches approximately that of the externally applied homogeneous field (3.3 T). At $\theta = 0°$, the field decreases monotonically as we move from the electrode to the bulk. This can be explained by the fact that the wire focuses the magnetic field,[14] and based on the continuity of $\boldsymbol{B}$ near the electrode, the field flux density is the sum of the external homogeneous field and the field induced by the magnetization of the wire. At $\theta = 90°$, the variation of $|\boldsymbol{B}|$ is very different. $|\boldsymbol{B}|$ is again high at the base of the wire (i.e., the electrode surface), but first it drops suddenly to a value lower than the flux density of the surrounding homogeneous field, and then it gradually increases again until it reaches the external field flux density. Though this behavior can be explained from the boundary conditions of the magnetic field at the surface of the wire,[23] magnetic field plots in this orientation are not readily available in the literature. Thus, based on the fact that with the wire oriented at $\theta = 90°$ the tangential component of the magnetic field intensity, $H_{||}$, is continuous at the base of the cylinder,[23] it is derived (based on $\boldsymbol{B} = \mu\boldsymbol{H}$) that $\mathbf{B}_{||,out} = \mu_{r,out}/\mu_{r,Fe}\mathbf{B}_{||,Fe}$, where $\mu_{r,out}$ and $\mu_{r,Fe}$ are

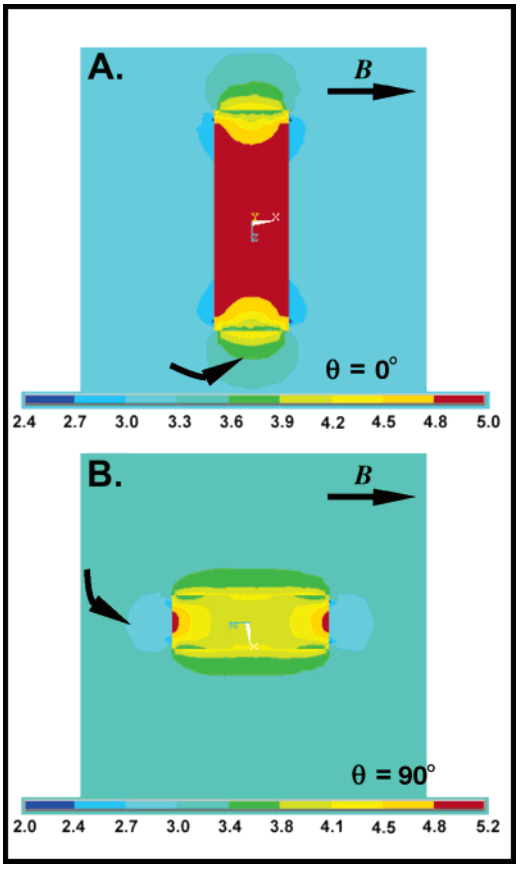

Figure 6. Magnetic field contour plots calculated with ANSYS: (A) at $\theta = 0°$ and (B) at $\theta = 90°$. Straight arrows represent the direction of the external applied magnetic field. Curved arrows show the side of the wire that is exposed to the solution and plays the role of the electrode. Values corresponding to the color coding are given within the figure in Tesla.

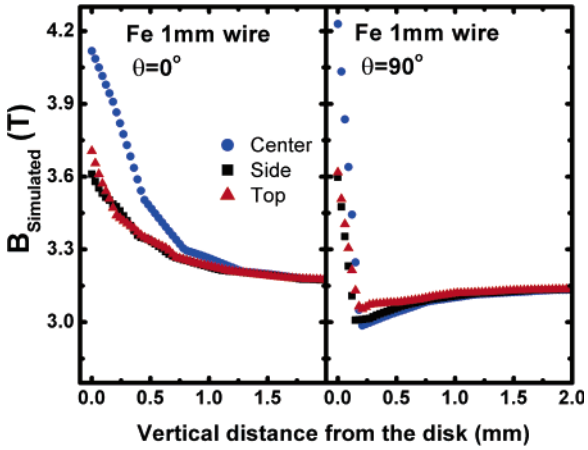

Figure 7. Magnetic field flux density, $\boldsymbol{B}$, as a function of distance from the disk electrode surface (from ANSYS data) (A) at $\theta = 0°$ and (B) at $\theta = 90°$. ('Center' refers to at the center of the disk; 'side' refers to the two edges at the two ends of a horizontal diameter; and, 'top' refers to the two edges at the two ends of a vertical diameter.)

the relative permeabilities of the two media cross the interface. Given that $\mu_{iron} = 5000$ and $\mu_{air} = 1.00$,[24] it is estimated that $[|\boldsymbol{B}|_{\parallel,\text{just outside}}/|\boldsymbol{B}|_{\parallel,\text{just inside Fe}}]_{at\ \theta=0} \approx 2 \times 10^{-4}$, and therefore the magnetic flux density reaches low values near the surface of the electrode compared to the bulk (3.3 T). (Given the physical size of the system, the resolution of the mesh used for the calculations in Figures 6 and 7 was not high enough to capture the exact values.) Importantly, according to Figure 7, the minimum $|\boldsymbol{B}|$ value is reached at around 0.2 mm from the surface of the 1 mm electrode, i.e., well within the diffusion layer (vide ante), and the field gradient is estimated at $\sim 5 \times 10^4$ T^2 m^{-1}. The implications of this statement in terms of defining the mechanism cannot be overemphasized. But first let us point out that in order to explain the OCP behavior at both extreme orientations ($\theta = 0°$ and $\theta = 90°$), it is key to appreciate the fact that corrosion starts from the moment the electrode is placed in the solution, thereby the magnetic field is imposed on already established (albeit continuously evolving) concentration profiles. Thus, at $\theta = 0°$, the corrosion process (eqs 1−3) creates higher concentrations of M^{2+} and Co^{II} near the electrode, fading (due to diffusion) away toward the bulk. By imposing on those concentration profiles a magnetic field that also fades away toward the bulk, we hold M^{2+} and Co^{II} back through the third term of eq 5. This increases their surface concentration and lowers the OCP (eq 4). At $\theta = 90°$, the magnetic field is again imposed on established concentration profiles, but most M^{2+} and Co^{II} lie in the region where it is favorable for them, due to the shape of the field, to move toward the bulk. That sink of M^{2+} and Co^{II} accelerates their diffusion away from the electrode, causing the rapid rise of the OCP (eq 4). Nevertheless, in the meantime, corrosion of M continues and all new M^{2+} and Co^{II} that are produced find themselves initially within the region (<0.2 mm) where the field is attracting. Thus after the rapid rise, the OCP shows a slow decrease created by accumulation of new Co^{II} and M^{2+} until a new steady state is reached controlled by a balance of diffusion out, magnetophoresis in, and magnetophoresis out.

The validity of this mechanism is predicated upon processes that involve higher concentrations of paramagnetic species near ferromagnetic electrodes. From this perspective, corrosion is just the supplier of paramagnetic species. Therefore, the same phenomena should be observable if high concentrations of radicals were formed independently of corrosion near the same ferromagnetic electrodes. This information would comprise confirming evidence for the so far implicit deconvolution of possible magnetic effects on the corrosion process (eq 1−3), from magnetic effects on mass transfer (eq 5) under conditions where the susceptibility increases from the bulk toward the electrode.

3.7. Deconvolution of the Solution-Phase Processes from Corrosion: Supporting Evidence for Magnetophoresis based on OCP Measurements with Nitrobenzene Radicals at the Electrode−Solution Interface. We worked with a 0.1 M nitrobenzene (NB) solution in CH_3CN/0.5 M TBAP and two bent disk-electrodes (Pt and Fe) at $\theta = 0°$ and $\theta = 90°$. The potential of the electrode was held at −0.8 V vs Ag/AgCl and was stepped for 10 s to −1.3 V. The whole potential range of the experiment is more negative than the redox potential of the Fe electrode, so neither electrochemical nor chemical corrosion of the Fe electrode by electrogenerated $NB^{\bullet -}$ was expected. After potential control was turned off, the OCP of each electrode was monitored both in the presence and absence of $\boldsymbol{B}$, and the results are presented in Figure 8. We notice that, in the case of the Pt electrode, the OCP increase is identical both in the presence and absence of the magnetic field at both orientations. In the case of the Fe electrode, we observe that at $\theta = 0°$, the increase of the OCP is slower in the presence of the magnetic field, while at $\theta = 90°$ the OCP increase is accelerated.

Our microscopic interpretation of these observations is as follows: during the 10 s potential step we create a layer of paramagnetic nitrobenzene anion radicals, $NB^{\bullet -}$, whose concentration is the highest at the electrode. After electrolysis, NB diffuses toward the electrode and electrogenerated $NB^{\bullet -}$ diffuses

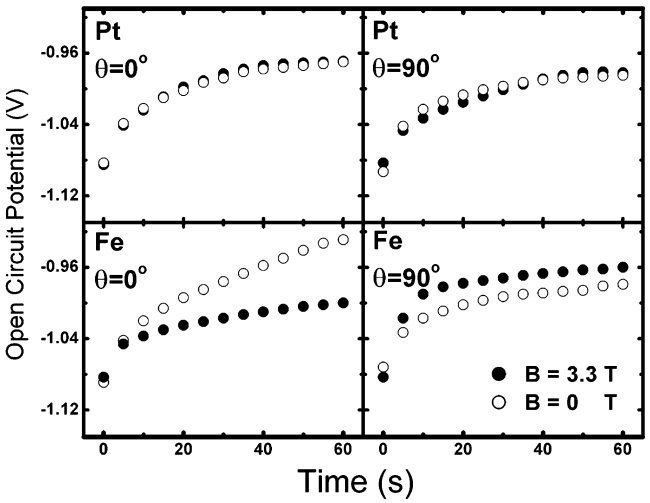

Figure 8. OCP decay with and without magnetic field (3.3 T) of 1.0 mm diameter bent Fe and Pt electrodes in CH_3CN/0.5 M TBAP solutions containing 0.1 M nitrobenzene. The observation of the OCP decay followed 10 s potential steps in order to accumulate nitrobenzene radicals, $NB^{\bullet-}$, in the vicinity of the electrodes. The experiments were repeated at two different orientations of the electrodes (refer to Scheme 1).

out, so that, based on the Nernst equation, the potential increases with time. The *slower* potential increase at $\theta = 0°$ with $\boldsymbol{B}$ 'on' is interpreted by the fact that $NB^{\bullet-}$ is held close to the electrode; the *faster* potential increase at $\theta = 90°$ and $\boldsymbol{B}$ 'on' is interpreted by the fact that $NB^{\bullet-}$ is pushed away from the vicinity of the electrode. The similarity between these results and those obtained during corrosion of Fe, Co, and Ni, supports the view that the magnetic effects on the corrosion of these metals under our conditions, are due to solution processes only.

4. Conclusions

Corrosion of ferromagnetic metals by the Wagner−Traud mechanism is sensitive to magnetic fields due to modification of the mass transfer mode of paramagnetic participants in the process. In the system considered for this study, the susceptibility of the solution is higher at the surface of the metal than in the bulk, and the magnetic effects have been traced to field-gradient driven mass transport of magnetic dipoles (magnetophoresis). In this context, previously unnoticed phenomena where the *direction* of the OCP change depends on the orientation of the electrode relative to the magnetic field have been simply associated with the shape of the magnetic field at those orientations. Although magnetohydrodynamic kind of convention is not present here, it should not be ruled out in systems that undergo corrosion by the local-cell mechanism.[1b]

Acknowledgment. We thank Joshua Williams for his assistance with the ANSYS™ simulations.

Supporting Information Available: Composition of the model for magnetic field simulations using ANSYS. Control experiments showing that the open circuit potential measuring device does not draw current through the solution. This material is available free of charge via the Internet at http://pubs.acs.org.

Appendix: Derivation of Equation 4

Let us consider an electrochemical cell whose reaction is a generalized form of eqs 1−3:

$$M + 2Co^{III} + 2e(Cu') \rightleftarrows M^{2+} + 2\,Co^{II} + 2e(Cu) \quad (A.1)$$

where M is Fe, Co, or Ni and Co^{II} and Co^{III} are the two redox forms of the couple $[Co(bipy)_3]^{3+/2+}$.

At equilibrium, electrochemical potentials, $\bar{\mu}$, and magnetoelectrochemical potentials, $\bar{\bar{\mu}}$, satisfy A.2:

$$\bar{\mu}_M{}^M + 2\bar{\mu}^s_{Co^{III}} + 2\bar{\mu}_e^{Cu'} = \bar{\bar{\mu}}^s_{M^{2+}} + 2\bar{\bar{\mu}}^s_{Co^{II}} + 2\bar{\mu}_e^{Cu} \quad (A.2)$$

and therefore

$$2(\bar{\mu}_e^{Cu'} - \bar{\mu}_e^{Cu}) = \bar{\bar{\mu}}^s_{M^{2+}} + 2\bar{\bar{\mu}}^s_{Co^{II}} - 2\bar{\mu}^s_{Co^{III}} - \bar{\mu}_M{}^M \quad (A.3)$$

For paramagnetic species (Fe^{2+}, Co^{2+}, Ni^{2+}, and Co^{II}), the magnetoelectrochemical potential, $\bar{\bar{\mu}}^s_{M^n}$, is given by

$$\bar{\bar{\mu}}^s_{M^n} = \bar{\mu}^s_{M^n} - Q_{M^n}|\boldsymbol{B}|^2 \quad (A.4)$$

where $Q_{M^n} = N_A[(m^*)^2/kT]$ (for definitions see ref 7).

Expanding the left-hand side of eq A.3, we obtain

$$2(\bar{\mu}_e^{Cu'} - \bar{\mu}_e^{Cu}) = -2FE \quad (A.5)$$

Expanding the right-hand side of eq A.3 we obtain

$$\mu^{0,s}_{M^{2+}} + RT\ln a^s_{M^{2+}} + 2F\Phi^s - Q_{M^{2+}}|\boldsymbol{B}|^2 + 2\mu^{0,s}_{Co^{II}} + 2RT\ln a^s_{Co^{II}} + 4F\Phi^s - 2Q_{Co^{II}}|\boldsymbol{B}|^2 - 2\mu^{0,s}_{Co^{III}} - 2RT\ln a^s_{Co^{III}} - 6F\Phi^s - \mu^{0,M}_M \quad (A.6)$$

Rewriting eq A.3 using eqs A.5 and A.6 we obtain

$$-2FE = -2FE^0 - RT\ln\frac{(a^s_{Co^{III}})^2}{(a^s_{Co^{II}})^2(a^s_{M^{2+}})} - Q_{M^{2+}}|\boldsymbol{B}|^2 - 2Q_{Co^{II}}|\boldsymbol{B}|^2 \quad (A.7)$$

where: $\Delta G° = \mu^{0,s}_{M^{2+}} + 2\mu^{0,s}_{Co^{II}} - 2\mu^{0,s}_{Co^{III}} - \mu^{0,M}_M = -2FE^0$.

Equation A.7 can be rewritten as eq 4:

$$E = E^0 + \frac{RT}{2F}\ln\frac{(a^s_{Co^{III}})^2}{(a^s_{Co^{II}})^2(a^s_{M^{2+}})} + \frac{Q_{M^{2+}}}{2F}|\boldsymbol{B}|^2 + \frac{Q_{Co^{II}}}{F}|\boldsymbol{B}|^2 \quad (4)$$

References and Notes

(1) (a) Bockris, J. O'M.; Reddy, A. K. N. *Modern Electrochemistry*; Plenum Press: New York, 1970; Vol. 2, pp 1346−1347. (b) Bockris, J. O'M.; Reddy, A. K. N. *Modern Electrochemistry*; Plenum Press: New York, 1970; Vol. 2, pp 1273−1275.

(2) Gross, W. *Verh. Dtsch. Phys. Ges.* **1885**, 38.

(3) Koenig, F. O.; Grinnell, S. W. *J. Phys. Chem.* **1942**, *46*, 980−1005.

(4) For example refer to: Bucherer, A. H. *Ann. Physik* **1896**, *58*, 564.

(5) Yamanoto, I.; Yamaguchi, M.; Goto, T.; Miura, S. *Sci. Rep. Res. Inst., Tohoku University, Ser. A* **1996**, *42*, 309−313.

(6) Leventis, N.; Gao, X. *Anal. Chem.* **2001**, *73*, 3981−3992.

(7) Assuming magnetization conditions far from saturation and that j is a free radical with spin S and charge z_j; N_A is Avogadro's number, k the Boltzmann constant, T the absolute temperature and m^* is defined by $m^* = gS\mu_B$, where g is the spectroscopic splitting factor, and μ_B the Bohr magneton.

(8) Waskaas, M. *Acta Scand.* **1996**, *50*, 516−520.

(9) (a) Waskaas, M.; Kharkats, Y. I. *J. Phys. Chem. B* **1999**, *103*, 4876−4883. (b) Waskaas, M.; Kharkats, Y. I. *J. Electroanal. Chem.* **2001**, *502*, 51−57.

(10) Cotton, F. A.; Wilkinson, G. *Advanced Inorganic Chemistry: A Comprehensive Text*, 4th ed.; John Wiley and Sons, New York, 1980; p 757.

(11) The comproportionation reaction $Fe^{3+} + Fe \rightarrow 2Fe^{2+}$ replaces one mole of Fe^{3+}, with magnetic moment of 5.9 μ_B, with 2 moles of Fe^{2+} with magnetic moment of 5.2 μ_B;[10] hence, the susceptibility of the solution should be higher at the electrode, decreasing toward the bulk.

(12) Perov, N. S.; Sheverdyaeva, P. M.; Inoue, M. *J. Appl. Phys.* **2002**, *91*, 8557−8559.

(13) Hinds, G.; Rhen, F. M. F.; Coey, J. M. D. *IEEE Trans. Magnet.* **2002**, *38*, 3216−3218.

(14) (a) Grant, K. M.; Hemmert, J. W.; White, H. S. *Electrochem. Commun.* **1999**, *1*, 319−323. (b) Pullins, M. D.; Grant, K. M.; White, H. S. *J. Phys. Chem. B* **2001**, *105*, 8989−8994.

(15) For a treatment of the subject refer to: (a) Leventis, N.; Gao, X. *J. Am. Chem. Soc.* **2002**, *124*, 1079−1088. (b) Leventis, N.; Dass, A. *J. Am. Chem. Soc.* **2005**, *127*, 4988−4989.

(16) (a) Jones, D. A. *Principles and Prevention of Corrosion*, 2nd ed.; Prentice Hall, NJ, 1996. (b) Trethewey, K. R.; Chamberlain, J. *Corrosion for Students of Science and Engineering*; Longman Group: UK, 1998.

(17) Yu, Q.-K.; Miyakita, Y.; Nakabayashi, S.; Baba, R. *Electrochem. Commun.* **2003**, *5*, 321−324.

(18) For example see: Suwa, M.; Watarai, H. *Anal. Chem.* **2001**, *73*, 5214−5219 and references therein.

(19) (a) Leventis, N.; Chen, M.; Gao, X.; Canalas, M.; Zhang, P. *J. Phys. Chem. B* **1998**, *102*, 3512−3522. (b) Burstall, F. H.; Hyholm, R. S. *J. Chem. Soc.* **1952**, 3570.

(20) Leventis, N.; Oh, W. S.; Gao, X.; Rawashdeh, A.-M. M. *Anal. Chem.* **2003**, *75*, 4996−5005.

(21) Fe wires of 0.25, 0.5, 1.0, and 2.0 mm diameter (Puratronic, 99.995%); Ni wires of 1.0, 2.0 (Puratronic, 99.999%) and 0.5, mm diameter, (Aldrich, 99.99+%); Co wires of 0.25, 0.5, 1.0, and 2.0 mm diameter (Puratronic, 99.995%), Pt wire of 1.0 mm diameter (Premion, 99.997%), Au wire of 1.0 mm diameter (Premion, 99.999%), and Zn wire of 1.0 mm diameter (Puratronic, 99.9985%).

(22) (a) Laitinen, H. A.; Kolthoff, I. M. *J. Am. Chem. Soc.* **1939**, *61*, 3344. (b) Bard, A. J.; Faulkner, L. R. *Electrochemical Methods Fundamentals and Applications*, 2nd ed.; John Wiley and Sons, New York, 2001; p 316. (c) Bard, A. J.; Faulkner, L. R. *Electrochemical Methods Fundamentals and Applications*, 2nd ed.; John Wiley and Sons, New York, 2001; pp 808−810. (d) Bard, A. J.; Faulkner, L. R. *Electrochemical Methods Fundamentals and Applications*, 2nd ed.; John Wiley and Sons, New York, 2001; p 147.

(23) (a) Hayt, W. H., Jr. *Engineering Electromagnetics*, 4th ed.; McGraw-Hill NY, 1981, pp 316−317. (b) Jackson, J. D. *Classical Electrodynamics*, 3rd Edition; John Wiley & Sons, New York, N.Y. 1999; p 194.

(24) Marshall, S. V.; Skitek, G. G. *Electromagnetic Concepts and Applications*, 3rd ed.; Prentice Hall, Englewood Cliffs, NJ, 1990; p 267.